ELSEVIER

Mechanical properties of SiO$_x$ gas barrier coatings on polyester films

D.G. Howells [a], B.M. Henry [a], Y. Leterrier [b], J.-A.E. Månson [b], J. Madocks [c], H.E. Assender [a],*

[a] *Department of Materials, University of Oxford, Parks Road, Oxford, OX1 3PH, UK*
[b] *Laboratoire de Technologie des Composites et Polymères (LTC), Ecole Polytechnique Fédérale de Lausanne (EPFL), CH-1015 Lausanne, Switzerland*
[c] *General Plasma, Inc, 546 E. 25th Street, Tuscon, Arizona 85713, United States*

Abstract

This paper reports the impressive mechanical properties of 1 μm thick carbon-containing SiO$_x$ gas barrier coatings, characterised using the uniaxial fragmentation test. Such coatings have been found to act as excellent barriers to water vapour permeation partly because they can be made so thick without stress induced cracking. The impressive mechanical properties are thought to be due in part to the high amount of carbon they contain, which gives them a more organic character, as well as the fact that they are deposited as a succession of thinner layers. The adhesion of the coatings to the polyester film is good in all cases, reflecting a high density of covalent bonding at the interface. Improvement of the mechanical properties of a SiO$_x$/PET composite can be achieved by altering the substrate. By replacing the PET with a heat-stabilised (HS) PET film, a HS film with an acrylate layer or PEN, it is found that the coating displays improved mechanical properties and adhesive strength (as well as barrier). This is thought to be due to the superior surface thermal and mechanical properties of these substrates. Deposition temperatures are at least 80 °C, which causes molecular motion at the surface of a plain PET film and creates defects in the SiO$_x$ coating as it grows, making it more brittle and permeable to gas flow.
© 2008 Elsevier B.V. All rights reserved.

Keywords: Gas barrier; Polyester; SiO$_x$; PECVD

1. Introduction

Silicon oxide coatings have proven to be useful in improving the gas barrier properties of plastic packaging, often reducing the permeation of oxygen and water through polymer film by 100 times or more [1]. Such composites have several advantages over traditional metallised polymer films, such as transparency and microwave compatibility. To achieve a long-term barrier to gas permeation, these coatings must be resilient and durable enough so that they can withstand the stresses that are applied to the composite during its lifecycle [2]. To this end a number of studies have been performed to assess the mechanical properties of these films and the adhesion to the substrate [3–7]. For plasma-enhanced chemical vapour deposited (PECVD) SiO$_x$ films (7–150 nm thick) it has been found that such layers are under minimal compressive internal stress and that they display excellent adhesion to PET films. Thicker coatings have been found to be more prone to failure than thinner ones at low strain

[7] due to the increased probability of large defects being present. Yanaka et al. [8] find that for evaporated silicon oxide, thicker coatings have lower tensile strength and are under less compressive strength due to stress induced cracking.

Previously, PECVD SiO$_x$ coatings containing some carbon deposited on polyester film with excellent barrier against water vapour permeation were reported [9] (See Table 1). These coatings are unusually thick for such an application and their high barrier properties suggest they have favourable mechanical properties. In this study we assess the mechanical properties of the silica and its adhesion to the polyester substrates using the uniaxial fragmentation test [2]. We also demonstrate that the choice of substrate can considerably influence the properties of the coating. As well as standard biaxially drawn PET, filled PET (F-PET), heat-stabilised[1] PET (HS PET), heat-stabilised PET with an additional primer layer (HS PET_P) and poly(ethylene naphthalate) (PEN) are all investigated as substrates.

---

* Corresponding author. Tel.: +44 1865 273781; fax: +44 1865 273789.
E-mail address: hazel.assender@materials.ox.ac.uk (H.E. Assender).

[1] Heat-stabilised films have been annealed under tension, which results in a more dimensionally stable product.

Table 1
Water vapour transmission rates (WVTR) for thick SiO_x coatings on polyester film (data taken at 50 °C using a MOCON permatran)

Substrate	Coating thickness (nm)	WVTR (substrate) $g\ m^{-2}\ day^{-1}$	WVTR (coated) $g\ m^{-2}\ day^{-1}$	BIF [a]
PET	400	9.80	0.20	49
F-PET	1000	14.95	0.09	167
HS PET	1000	7.47	<0.01	>750
HS PET_P	1000	7.47	<0.01	>750
PEN	1000	3.02 (0.37) [b]	<0.01 (2×10^{-4}) [c]	>300(~1900) [c]

[a] Barrier improvement factor — the ratio of WVTR (substrate) and WVTR (coated).

[b] Value at 20 °C (extrapolated using activated rate theory [10] for WVTR data obtained at 30, 40 and 50 °C).

[c] Data obtained at 20 °C using an isotopic mass spectroscopy method [11].

The thickness of the SiO_x examined is 1 μm as this was shown to possess the highest barrier to water vapour permeation. In an earlier report a 1 μm thick coating was found to have poor barrier and mechanical properties on a standard PET film [9], so a 400 nm coating on this substrate was investigated here instead.

2. Theory

A useful measure of coating strength is the maximum cohesive strength of the SiO_x fragments at saturation, σ_{max}, as this value is required to measure the adhesive strength of the coating/polymer interface. However, at saturation the fragment length is too small to measure its strength directly. Nevertheless it can be modelled using the Weibull distribution for the probability of failure of ceramics, based on the idea that failure at any flaw leads to total failure of the material [5, 12, 13]. The strength of coating fragments depends on the probability of having a critical size defect, which for a uniform defect distribution is related to the volume (i.e. length) of coating under stress. The probability of failure, P_f, of a specimen can be expressed by:

$$P_f = 1 - \exp\left[-\frac{l}{l_0}\left(\frac{\sigma}{\beta}\right)^\alpha\right] \qquad (1)$$

Following from this, in the initial stages of fragmentation, the average fragment length, $<l>$, (in μm) at small strains can be expressed as [5]:

$$<l> = l_0(\sigma/\beta)^{-\alpha} \qquad (2)$$

l_0 is a normalising factor of 1 μm, σ is the axial stress in the coating and α and β are the Weibull shape and scale factors respectively. α and β can then be extracted from a plot of ln $<l>$ against ln σ. α is known as the shape parameter or Weibull modulus and is an indication of the distribution of failure stresses — a higher value represents a narrow distribution and a higher reliability. β is a normalising factor, often termed the scale parameter.

With the parameters α and β the coating strength at critical length is given by:

$$\sigma_{max}(l_c) = \beta(l_c/l_0)^{-1/\alpha}\cdot\Gamma(1+1/\alpha) \qquad (3)$$

Where Γ is the gamma function. The critical length is the smallest fragment that can undergo failure and is related to the average fragment length at saturation ($<l_{sat}>=1/CD_{sat}$) by $l_c = 1.5<l_{sat}>$ following a detailed analysis of the fragment length distribution in SiO_x on PET [5].

In the presence of internal stresses the crack onset strain (COS) and coating strength determined by this method is an observed, apparent measure of the coating properties. We correct for compressive strain inherent in the coating before testing because upon fragmentation the average coating stress relaxes, as the average stress in the fragments decreases when their size decreases. Assuming a constant shear stress we get [14, 2]:

$$COS^* = COS + \varepsilon_i \qquad (4)$$

$$\sigma_{max}^*(l_c) = \sigma_{max}(l_c) + 0.67\sigma_i \qquad (5)$$

where COS* is the intrinsic crack onset strain, $\sigma_{max}^*(l_c)$ is the intrinsic cohesive strength and ε_i and σ_i are the internal strain and stress respectively (negative for compression). The factor 0.67 results from the relaxation of the stress at the fragment edges [15]. Throughout this work the * refers to the intrinsic property, after internal stresses have been accounted for.

The adhesion between the coating and polymer, defined as the interfacial shear strength (IFSS), τ, is derived from the CD at saturation (and therefore l_c) following an adapted version of the Kelly–Tyson model [5, 16] which assumes a perfectly plastic interface and therefore a constant IFSS and was originally developed for fibre-reinforced materials (the fibre is analogous to the coating and the matrix is analogous to the polymer substrate). Important aspects of this model are that the applied load is transferred from the polymer to the coating by means of shear forces at the interface, thereby stretching the coating and that these are limited by the shear yield stress of the polymer or by the shear strength of the interface (whichever is lower). Plastic flow of the substrate and the flow stress are greatest beneath the cracks and the fragment edges and a higher crack count (low fragment length) signifies a larger interfacial shear strength.

The force acting over an infinitesimally small length of coating, dx (Fig. 1), of thickness h_c, can be expressed as [17]:

$$\frac{d\sigma_x}{dx} = \frac{\tau}{h_c} \qquad (6)$$

Hence:

$$\tau = 2h_c\sigma_{max}(l_c)/l_c \qquad (7)$$

The intrinsic interfacial shear strength, τ^*, is then simply given by:

$$\tau^* = 2h_c\sigma_{max}^*(l_c)/l_c \qquad (8)$$

3. Experimental methods

Fabrication of the barrier layers was performed by General Plasma, Inc. (Tuscon, USA) who used a pilot roll-to-roll coater
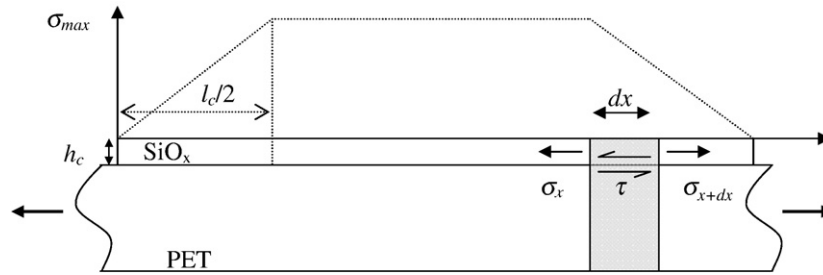
Fig. 1. Schematic representation of the stress transfer between PET and a section of SiO$_x$ coating between the cracks when the composite is under tensile load.

with a web width of 150 mm to deposit PECVD SiO$_x$ layers using their high density PDP source technology [18]. Prior to deposition, the films were plasma treated using nitrogen gas, with a flow rate of N$_2$ of 50 sccm and a power of 200 W at web speed 0.6 m min^{-1}. To deposit 1 μm thick SiO$_x$ films, precursor gases hexamethyldisiloxane (HMDSO) and oxygen were used at a flow rate of 75 sccm and 30 sccm respectively at a power of 300 W, and a pressure of 20 mTorr. The web speed was 0.2 m min^{-1} and a total of six passes were performed to achieve the required thickness. There is no known compositional difference between successive layers. The morphology that arises from these multiple passes is thought to influence the resulting barrier properties [19]. For the 400 nm layer on PET the web speed was 0.33 m min^{-1} and four passes were made. The thickness of the coatings was determined by profilometry and UV–visible spectroscopy by the manufacturers.

The substrates were 125 μm thick poly(ethylene terephthalate) (PET) and poly(ethylene 2,6-naphthalate) (PEN) films, 175 μm thick heat-stabilised (HS) PET and primer-coated HS PET. The primer layer is a thermally crosslinked terpolymer of three acrylate monomer species, and is designed to improve adhesion of layers to the film. The major constituents are ethyl acrylate (EA) and methylmethacrylate (MMA). Also investigated was a 75 μm thick PET film with 0.21 wt.% of china clay (aluminium silicate) filler particles (F-PET). AFM analysis revealed a mean particle diameter at the surface between 1.4 and 1.7 μm with 4000 particles mm^{-2}. The particles are added as "antiblocking" agents to prevent the adherence of the film to itself in the roll, by reducing the surface area of contact between adjacent layers. Deposition was attempted on a film consisting of coextruded semicrystalline PET and amorphous PET but this suffered severe thermal shrinkage due to relaxation in the amorphous material and was neglected in this study. All of the films were supplied by DuPont Teijin Films (DTF).

X-ray photoelectron spectroscopy (XPS) analysis found that the silica is sub-stoichiometric at SiO$_{1.8}$ and the coatings were estimated to contain 18–25% carbon by atomic composition. A small absorption in the UV–visible region between 320 and 450 nm is observed for the SiO$_x$. The refractive index of the SiO$_x$ was found to be 1.6, a value higher than the standard of 1.46 for SiO$_2$ which again may be a consequence of the sub-stoichiometry or the carbon content of the film.

For high resolution microstructural characterisation of the polyester film surfaces, a Digital Instruments Nanoscope Multimode atomic force microscope (AFM) was employed in Tapping Mode, with tip radius of less than 10 nm. A Park Scientific Instruments AFM was used for the force–distance measurements.

In-plane deposition-induced internal stresses, σ_i, were calculated using the radius of curvature of the films before, R_1, and after, R_2, deposition [2, 20]:

$$\sigma_i = \frac{E_s h_s^2}{6(1-v_s)h_c}\left(1+\frac{h_c}{h_s}\left(4\frac{E_c}{E_s}-1\right)\right)\left(\frac{1}{R_2}-\frac{1}{R_1}\right) \qquad (9)$$

E_s and E_c are the Young's moduli of substrate and coating respectively, v_s is the substrate Poisson's ratio and h_s and h_c are the respective thicknesses. Compressive stresses are denoted as being negative. The radii R_1 and R_2 of the samples supported freely on two vertical aluminium plates were measured with an Olympus SZH binocular lens. The Young's modulus of SiO$_x$ was assumed to be 80 GPa, following literature reports [6], the Young's modulus of the substrates were determined from tensile testing, and their Poisson's ratio was assumed to be 0.3 (manufacturer's data).

The mechanical and adhesive properties of the coating were examined using the fragmentation test, in which the onset and development of cracking of the brittle coating was monitored as a function of the applied uniaxial tensile load, *in-situ* under an optical microscope. Rectangular film specimens (approx 40 × 10 mm) underwent tensile loading in a computer controlled Minimat unit (Rheometric Systems) by means of a stepper motor (load 1000 N). This unit provides measurement of displacement within 1 μm accuracy. Accurate measurement of specimen strain was achieved by a non-contact video extensometry technique [21] in which the relative displacement between the centres of gravity of ink markers deposited onto the surface of the specimen was monitored by means of image processing tools during application of the load. This overcame problems such as possible slippage of the specimen in the clamps. Sandpaper was glued to the ends of the specimen in the clamps to minimise damage to the coating and slippage.

The tensile unit was placed under an optical microscope (Olympus BX60) for analysis. Cracking of the coating was analyzed at increasing strain levels in terms of crack density (CD), defined as the inverse of the average fragment length (*l*) and calculated from the average number of cracks, N_i, counted on k micrographs of width W, at strain ε, as

$$CD = (1+\varepsilon)\Sigma_{i=1}^{k} N_i / kW \qquad (10)$$

The factor $(1+\varepsilon)$ corrects for crack opening to the first approximation.

4. Substrate properties

The vacuum deposition of a coating on a substrate inevitably leads to high energy species bombarding the substrate and a subsequent heating, which for a polymer such as PET can affect its structure and morphology, particularly as the T_g is in the region 60–120 °C — similar to typical deposition temperatures. The value of surface T_g for PET and PEN has previously been reported [22, 23] but little is known about the thermal properties of amorphous acrylate layers. To get an idea of how a surface will behave during deposition, the surface T_g of a substrate can be estimated using force–distance measurements of an AFM tip approaching and leaving the surface as described by Bliznyuk et al. [24]. In this technique an AFM tip approaches the surface until it just embeds into the material. As it is removed the surface tension of the amorphous polymer causes hysteresis and the tip breaks free of the polymer at some distance from the original point of contact on the approach. Such a distance is known as the "snap off" distance and increases with temperature more rapidly above the T_g than below.

As shown in Fig. 2 for PET the T_g (for the amorphous regions in the semicrystalline film) is measured to be 80 °C, a higher value than expected from literature data of surface T_g in cast PET thin films [25], which is probably a result of the oriented nature of the amorphous regions and the constraining effect of the crystallites in the film [19, 26]. For the heat-stabilised film it was found that very few soft amorphous zones existed at the surface to perform these measurements and the tip was found to dissociate from the surface almost immediately upon retraction in most cases, evidence of an increased degree of surface crystallisation in this film. This was confirmed by AFM imaging (Fig. 3) which shows a rougher surface with discrete 20–30 nm features on the HS PET film compared to the plain PET that are most likely crystallites [27]. The surface T_g for PEN was found to be 120 °C — similar to bulk values reported previously [28].

For the amorphous primer layer the measured T_g is about 50 °C. There is a lot more scatter in the measured snap off distances, indicating non uniformity in local composition of the primer. The measured value seems sensible as it falls between
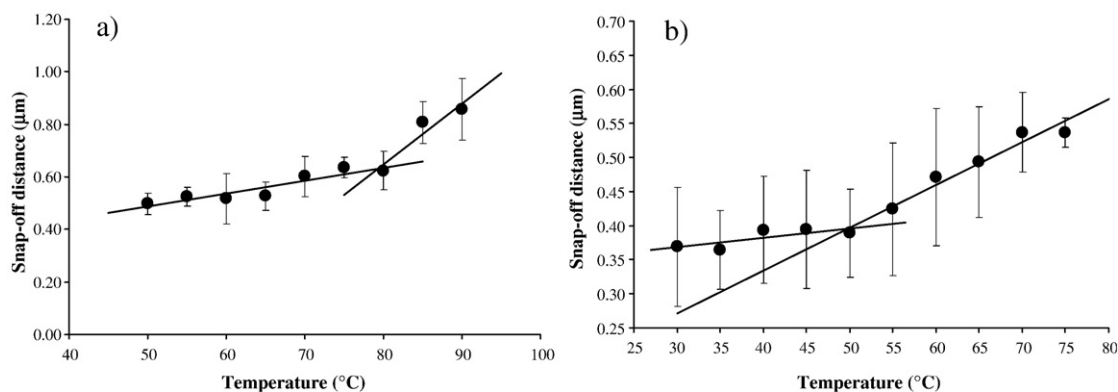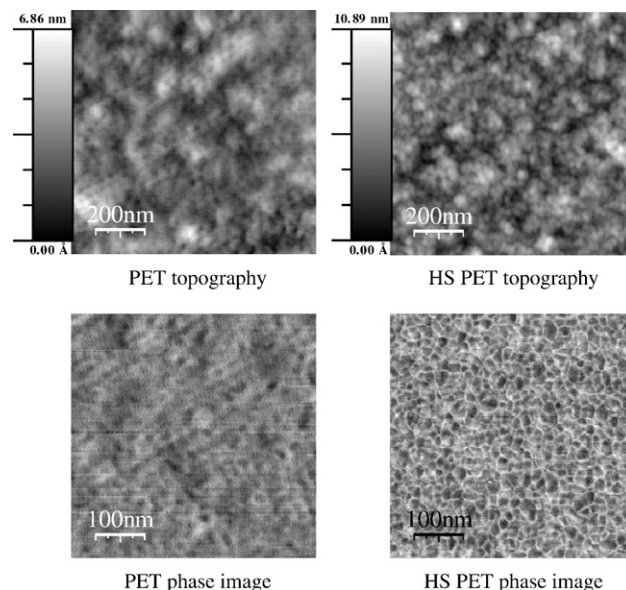

Fig. 3. AFM topography and phase images of (left) PET and (right) HS PET.

the T_g values for the homopolymers of the two major constituent monomers in the acrylate, which are −8 °C and 105 °C for PEA and PMMA respectively [29].

If during deposition the temperature of the polymer surface rises above T_g it is likely that there will be relaxation of the aligned amorphous chains and, for the polyester, crystallisation at the surface, which may influence the deposition of the coating in the early stages. This effect will be diminished in heat-stabilised film as the surface is already more crystalline and the amorphous segments already relaxed. Even though the T_g is lower for the primer layer than PET, because it is a crosslinked copolymer with little or no orientation, the chains will not relax significantly or crystallise in the temperature regime of deposition as is observed for PET. It is clear that the substrate does undergo high temperatures during deposition as a coextruded film with one layer of standard semicrystalline PET and another of amorphous PET was found to shrink dramatically during the coating process, due to relaxation of the oriented amorphous layer.

Fig. 2. Snap-off displacement v temperature curves for a) PET showing a T_g of 80 °C and b) acrylate primer on HS PET_P, with a T_g of 50 °C. In each case we performed a separate linear regression of the points above and below the surface T_g and repeated the process with different estimated surface T_g. The value that leads to the greatest regression coefficient is the quoted T_g [24].
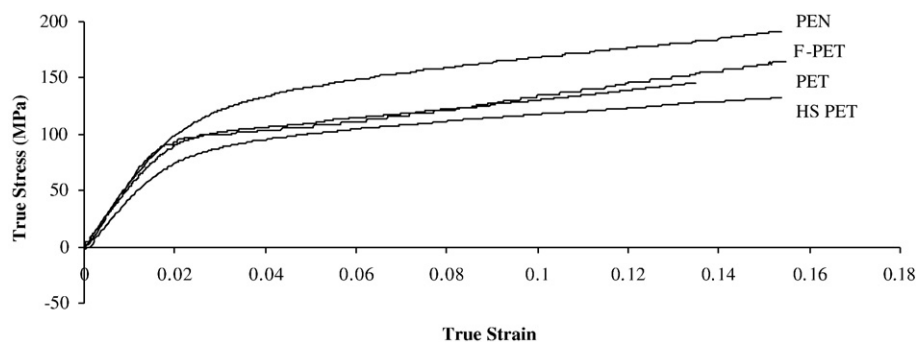
Fig. 4. True stress–strain curves for polyester films.

The mechanical properties of the polyester films were examined using tensile testing. True stress–strain curves (Fig. 4) were obtained for the strain regime relevant in the fragmentation test (not up to rupture) to give an idea of the polymer substrate behaviour in this region and a constant extension rate of 0.4 mm min^{-1} was employed, with the extension in the transverse direction of the film (that perpendicular to the processing axis (machine direction)). When considering the interfacial shear strength of the composite, the yield stress (Table 2) and behaviour of the substrate after yield are important factors because they can limit the value of τ if the interface is strong [2].

Both filled and unfilled PET film yields at about 100 MPa and 2.5% strain. Instead of pure plastic yield, these films show a small degree of strain hardening almost immediately after the yield point, due to their orientation and high crystallinity. The HS PET film is found to have inferior mechanical properties to the plain PET. It has a lower Young's modulus, a lower yield stress and appears to strain harden less in the strain regime examined here. The heat-stabilisation process involves heating the film at temperatures in Regime III described by Gohil [30] (in the region of 200 °C), which is expected to have two main effects on the structure of the film. The first is that metastable crystals melt and larger crystals form as a result of crystal growth and recrystallisation, leading to a net increase in the degree of crystallinity. The second is that the amorphous phase relaxes so that minimal shrinkage occurs during subsequent heating. This relaxed amorphous phase is then responsible for the lower modulus and yield stress as it must be reoriented under tension. The very high crystallinity observed at the surface by AFM is probably due to the fact that the T_g is lower at the surface leading to a higher degree of crystallisation there than in the bulk [31, 32]. Finally, as expected, PEN exhibits a greater modulus and yield stress. The improved properties are mainly due to the presence of the naphthalene ring in the PEN structure [28].

5. Results

5.1. Stress and mechanical strength

Images of the various stages of fragmentation of a 1 μm thick coating on HS PET are given in Fig. 5, showing crack onset at a defect followed by rapid cracking, crack widening and finally saturation at 12% strain. Transverse cracking (cracks parallel to direction of strain) are observed close to saturation, as a result of compressive buckling due to the transverse contraction of the substrate (Poisson's ratio effects). The fragmentation process can be summarised in a plot of crack density against applied tensile strain (Fig. 6).

Fig. 6 shows the different fragmentation characteristics for 1 μm-thick coatings on four substrates with the superior properties of the HS PET_P composite being noticeable. The coating on the F-PET substrate is seen to behave particularly poorly and even after stresses are accounted for is the weakest coating at that thickness. The internal stresses reported in Table 3 show that the highest value is observed for the plain PET substrate, which indicates that this substrate undergoes more thermal shrinkage than the other films. The PEN film has a higher T_g than PET and so has a lower value of stress as it does not undergo shrinkage, although it is surprising to see relatively large levels of stress in the heat-stabilised films. The low level of stress recorded for SiO_x on the F-PET film is difficult to explain and may be a result of very pronounced curvature in the machine direction (perpendicular to that of the measured transverse direction) that makes measuring the curvature in the TD difficult. It is unlikely to be due to stress induced cracking caused by the filler particles as the film is measured to be a good gas barrier.

Table 3 displays the data obtained from the fragmentation testing of the coated samples. Generally the properties are comparable to those of much thinner coatings reported in the literature [5, 7] and this may be due to the mechanism of depositing the coating in multiple layers (of ~ 167 nm for 1 μm thick SiO_x and ~100 nm for 400 nm SiO_x). Because these films are such good barriers it is likely that defects don't propagate through the film, so that the thickness produced by an individual pass controls the mechanical properties and the defect size [19].

Table 2
Mechanical properties of polyester films

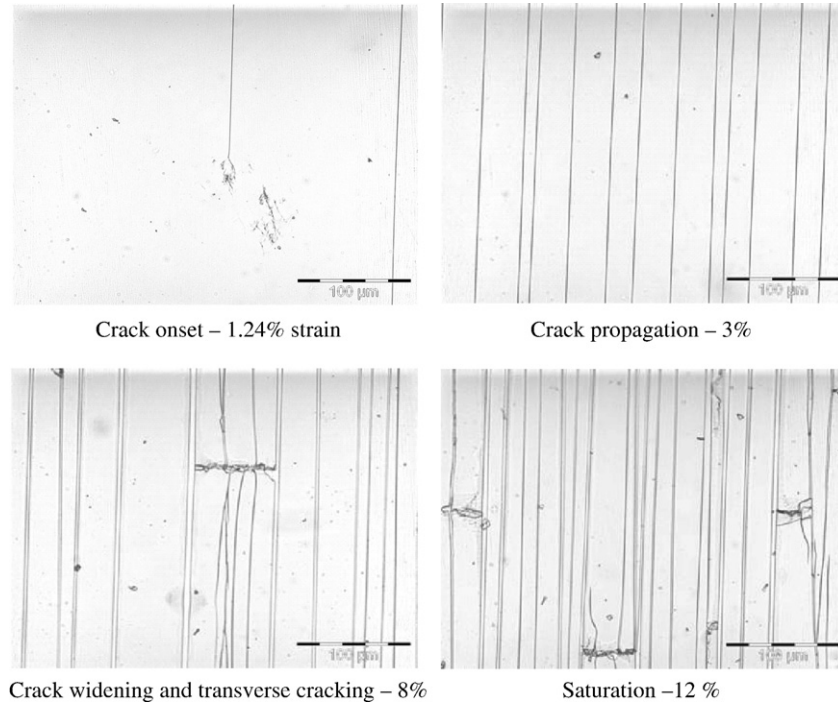| Substrate	E modulus (GPa)	Yield strain (%)	Yield stress (MPa)	% Thermal shrinkage (after 190 °C, 5 min)
PET	4.8	2.5	100	3
F-PET	5.3	2.5	100	1
HS PET	4.3	3.0	90	0.03
PEN	6.1	3.5	140	0.8

Fig. 5. Fragmentation process of a 1 μm thick SiO_x coating on HS PET film.

The initial layer is likely to have most defects due to the substrate roughness and polymer chain motion, therefore the strength of the 1000 nm thick coating is controlled by the initial 167 nm thick layer and the 400 nm SiO_x by that of the initial 100 nm layer. This explains the similarity in mechanical properties between these "thick" coatings and the thinner ones reported in the literature.

The effect of changing the parameters α and β on the cumulative distribution function (cdf) of probability of coating failure, $P(f)$ against tensile stress is illustrated in Fig. 7. A higher value of α narrows the failure range whereas an increase in β expands the cdf to the right, effectively increasing the average strength. The values of α are very similar for all 1 μm thick coatings and are indicative of a good quality ceramic material on each substrate. The much higher value observed for the 400 nm thick layer on PET is likely to be because thinner coatings have a narrower defect size distribution (i.e. a narrower range of failure stresses) and is not a substrate effect. Interestingly the values of β (the scale factor and an indicator of average strength) are much greater for the SiO_x layers on HS PET, HS PET_P and PEN than for those on PET and F-PET, which appear to be more prone to brittle failure.

Once internal stresses are accounted for there is a great difference in tensile strength between the coatings on the different substrates, with the SiO_x on plain PET being particularly poor despite being thinner than the rest. A pertinent factor may be the heating effect caused by deposition, which increases the temperature at the polymer surface to or above the region of the PET T_g. Such heating may cause relaxation of constrained amorphous chains and in addition could induce crystallisation at the surface. The molecular motion of polymer chains at the surface may be responsible for creating defects in the interfacial region, as their movement during deposition could move the initial deposits of silica laterally on the surface, leaving holes in the structure. Both barrier performance and mechanical strength depend on defects and it is no surprise that the worst barriers in this study have the weakest mechanical properties.
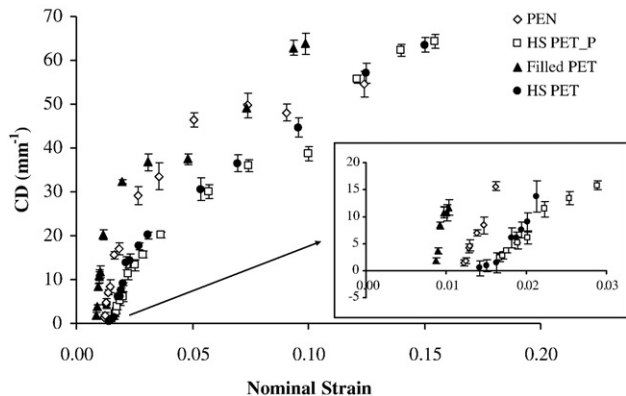

Fig. 6. Plot of crack density against nominal strain for 1 μm thick coatings on a variety of polyester substrates.

Table 3
Mechanical properties of SiO_x coatings on polyester films

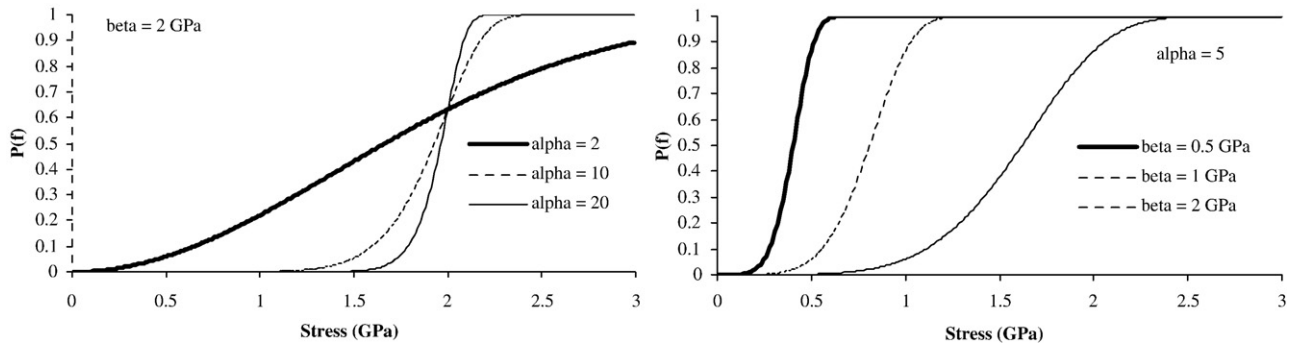|	PET	F-PET	HS PET	HS PET_P	PEN
σ_i, MPa	-648 ± 23	-78 ± 14	-483 ± 20	-517 ± 16	-195 ± 18
COS %	1.32 ± 0.12	0.92 ± 0.05	1.26 ± 0.16	1.61 ± 0.11	1.16 ± 0.06
COS* %	0.58 ± 0.11	0.85 ± 0.05	0.84 ± 0.15	1.16 ± 0.12	0.99 ± 0.06
A	23 ± 12	8 ± 3	10 ± 1	9 ± 2	8 ± 2
β, GPa	1.49 ± 0.11	1.65 ± 0.24	2.04 ± 0.57	2.44 ± 0.31	2.14 ± 0.47
$\sigma_{max}(l_c)$, GPa	1.05 ± 0.18	1.00 ± 0.03	1.39 ± 0.26	1.66 ± 0.11	1.3 ± 0.1
$\sigma_{max}(l_c)$*, GPa	0.77 ± 0.18	0.95 ± 0.02	1.07 ± 0.27	1.31 ± 0.12	1.17 ± 0.1

Fig. 7. The effect of alpha and beta on the cumulative distribution function for the probability of coating failure as a function of stress (for fragment length = 1 μm).

The heat-stabilised PET and PEN composites have superior properties compared to the PET and F-PET ones because they are more resistant to heat. PEN has a surface T_g of 120 °C and it is unlikely that the deposition temperature is high enough to cause chain motion at the surface. Similarly, the greater degree of crystallinity observed for the HS PET film, combined with the relaxed amorphous phase means that there will be much less chain relaxation and motion at the film surface. The best mechanical strength is observed for the SiO$_x$ on the HS PET_P film. Maybe, because the temperature of deposition is greater than the T_g of the acrylate, the surface of this film will be soft and allow the oxide to stick easily and form a dense layer without the acrylate molecules contracting and moving the initial SiO$_x$ deposits around. Because the acrylate chains are thoroughly crosslinked and relatively unoriented they are not expected to relax during deposition, despite the temperature being above the T_g of the primer (and the underlying PET is heat-stabilised, so neither layer is expected to shrink significantly on heating).

5.2. Adhesive strength

One of the assumptions of the Kelly–Tyson model of interfacial shear stress is that the stress experienced by the coating is from shear forces caused by bonds at the interface as the polymer yields beneath it and is limited by the strength of the interface or the strength of the polymer under shear, whichever is the weakest (plastifies first) [5, 16]. If the polymer substrate becomes completely plastic then no more stress can be transferred across the interface to cause further cracks and saturation will be observed.

It is therefore interesting to note that once internal stresses are accounted for, the intrinsic interfacial shear strength τ^* is found to be equal to, or greater than, the substrate shear yield stress for each composite (Table 4). The shear yield stress, τ_y, of the polymer is calculated using the Von Mises relationship [5] ($\tau_y = \sigma_y/\sqrt{3}$ where σ_y is the tensile yield stress of the polymer film, obtained using tensile testing). For coated polymers if τ^* is similar to the substrate shear yield stress then it is likely that the substrate is plastically yielding, causing the interface to plastify, meaning that for SiO$_x$ coatings there is a large density of Si–O–C and Si–C covalent bonds at the interface between polymer and silica, causing a strong bond. Therefore, as all the

values of τ^* are around or above the substrate shear yield stresses the adhesion, i.e. covalent bonding between the two layers, is excellent and any observed differences are due to the mechanical properties of the polymer. This is demonstrated for the PET and PEN samples where in each case the τ^* is comparable to the respective τ_y values and is consequently higher for the PEN composite although the extent of interfacial covalent bonding for each composite is probably similar. The effects of the substrate surface mechanical properties on the τ^* are summarised in Fig. 8.

The measured value of τ^* is much greater than the estimated shear yield stress of the substrate for the heat-stabilised PET film. This is most likely a result of the high degree of crystallisation detected at the surface by AFM phase and force–distance measurements, but which may not be present throughout the bulk. A high degree of crystallisation is known to increase the tensile yield stress (hence shear yield stress) of PET [33] and may also encourage strain hardening of the polymer. No elevated yield stress or strain hardening in the saturation regime (10–15% tensile strain) is observed for the HS PET film during tensile testing but this is probably due to the localisation of the increased crystallinity at the surface of the film, as reported in the literature [31, 32]. It appears that the crystalline surface morphology caused by heat treatment strengthens the polymer in the interfacial region allowing a superior τ^* to be observed that matches that of PEN. Similarly, the τ^* for filled PET is greater than that of the plain PET and the shear yield stress of the F-PET substrate — this could be explained by increased crystallinity at the surface of this film, as witnessed using AFM by other authors on similar films [34].

The addition of the primer layer to the HS PET causes the τ^* to increase to above 110 MPa and a much higher CD$_{sat}$ is observed for this composite. Such a high τ^* value could be due to the increased functionality of the primer surface (shown by

Table 4
Adhesive strength of SiO$_x$ coatings on polyester film

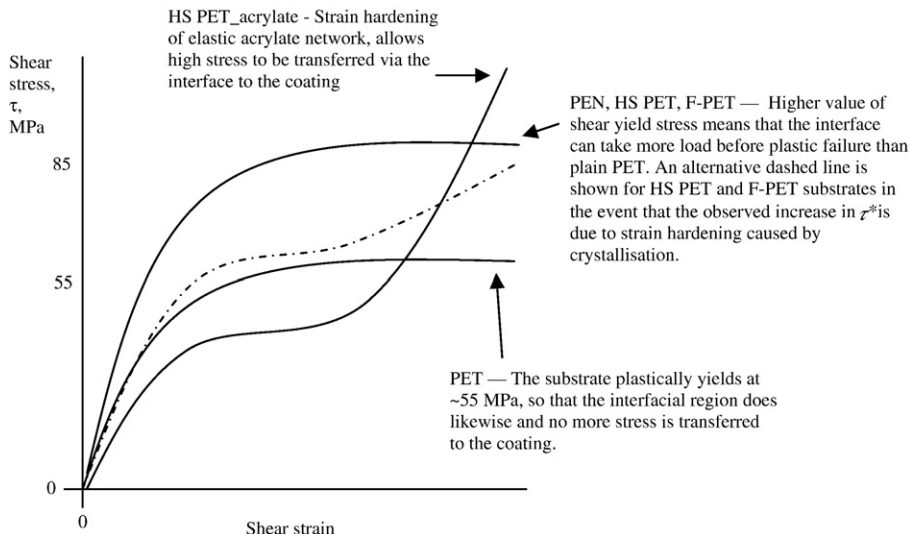| Substrate	CD$_{sat}$ mm^{-1}	τ (MPa)	τ^* (MPa)	τ_y, polymer (MPa)
PET	143±12	82±12	52±12	58±3
F-PET	63±2	84±4	79±4	58±3
HS PET	62±7	116±33	89±33	52±3
HS PET_P	69±15	152±24	120±18	52±3
PEN	55±8	94±10	85±9	80±3

Fig. 8. Schematic of the mechanical behaviour of the polyester substrates under shear, in the vicinity of the interface with the oxide coating.

XPS and water contact angle measurements) resulting in substantially increased covalent bonding at the interface, but the acrylate itself must also have superior mechanical properties.

In this case the acrylate is a terpolymer which contains mainly MMA (PMMA is a glassy polymer [29]) and ethyl acrylate (polyethylacrylate is an elastomer [35]) with a small amount of methacrylamide to facilitate crosslinking.

It is a possibility that the acrylate is elastomeric, which would explain why τ^* is so large. By considering the stress–strain behaviour of a highly crosslinked rubber (Fig. 8) it can be seen that the hardening observed for such a material at a higher strain would lead to a high value of τ^*. Much more work is required to confirm that elastomeric behaviour is exhibited for such thin acrylate films and that this is responsible for the high $\tau*$ observed but it seems to be the most reasonable explanation given the available data.

6. Conclusion

The work presented in this paper has demonstrated that 1 μm thick SiO_x coatings deposited on polyester film have impressive mechanical properties to match the excellent gas barrier performance reported previously. This is due to the high degree of carbon present in these films and the fact that they are deposited in multiple layers, so that defects do not extend throughout the thickness of the silica. The choice of substrate also influences the properties of the films — those deposited on PET and, to a lesser extent, filled PET are more brittle and prone to failure. Those deposited on PEN, HS PET and HS PET_P are superior and in the main this is because the surfaces of these substrates are less affected by the deposition temperatures that are above the PET T_g of 80 °C. For the PET and F-PET films it is likely that heating causes chain motion of the oriented amorphous phase, be it through relaxation or crystallisation. This has the effect of causing the initial deposits to move across the surface and creates defects, that are then responsible for a more permeable coating that fractures more easily.

References

[1] H. Chatham, Surf.Coat.Technol. 78 (1996) 1.
[2] Y. Leterrier, Prog. Mater. Sci. 48 (2003) 1.
[3] G. Rochat, A. Delachaux, Y. Leterrier, J.-A.E. Månson, P. Fayet, Surf. Interface Anal. 35 (2003) 948.
[4] G. Rochat, Y. Leterrier, C.J.G. Plummer, J.-A.E. Månson, R. Szoszkie-wick, A.J. Kulik, P. Fayet, J. Appl. Phys. 95 (10) (2004) 5429.
[5] Y. Leterrier, L. Boogh, J. Andersons, J.-A.E. Månson, J. Polym. Sci., B. Polym. Phys. 35 (1997) 1449.
[6] G. Rochat, Y. Leterrier, P. Fayet, J.-A.E. Månson, Thin Solid Films 484 (2005) 94.
[7] Y. Leterrier, J. Andersons, Y. Pitton, J.-A.E. Månson, J. Polym. Sci., B. Polym. Phys. 35 (1997) 1463.
[8] M. Yanaka, Y. Tsukahara, N. Nakaso, N. Takeda, J. Mater. Sci. 33 (1998) 2111.
[9] D.G. Howells, B.M. Henry, L. Medico, Y. Leterrier, J.-A.E. Månson, H.E. Assender, 48th Annual Technical Conference Proceedings of the Society of Vacuum Coaters., 2005.
[10] Y.G. Tropsha, N.G. Harvey, J. Phys. Chem., B. 101 (1997) 2259.
[11] H. Norenberg, G.D.W. Smith, G.A.D. Briggs, T. Miyamoto, Y. Tsukahara, 45th Annual Technical Conference Proceedings of the Society of Vacuum Coaters, 2002, p. 546.
[12] J.B. Wachtman, Mechanical Properties of Ceramics, Wiley, New York, 1996.
[13] W. Weibull, J. Appl. Mech. 18 (1951) 293.
[14] Y. Leterrier, Y. Wyser, J.-A.E. Månson, J. Adhes. Sci. Technol. 51 (2001) 841.
[15] A.C. Kimber, J.G. Keer, J. Mater. Sci. Lett. 1 (1982) 353.
[16] A. Kelly, W.R. Tyson, J. Mech. Phys. Sol. 13 (1965) 329.
[17] G. Rochat, Y. Leterrier, P. Fayet, J.A.E. Månson, Thin Solid Films 437 (2003) 204.
[18] J. Madocks, J. Rewhinkle, L. Barton, Mat. Sci. Eng., B. 119 (3) (2005) 268.
[19] D.G. Howells, B.M. Henry, J. Madocks, H.E. Assender Thin Solid Films In press.

[20] K. Roll, J. Appl. Phys. 47 (1976) 3224.
[21] Y. Leterrier, L. Medico, F. Demarco, J.-A.E. Månson, U. Betz, M.F. Escola, M. Kharazzi Olsosn, F. Atamny, Thin Solid Films 460 (2004) 156.
[22] S.M. Aharoni, Polym. Adv. Tech. 9 (1999) 169.
[23] Y. Zhang, J. Zhang, Y. Lu, Y. Duan, S. Yan, D. Shen, Macromolecules 37 (2004) 2532.
[24] V. Bliznyuk, H.E. Assender, G.A.D. Briggs, Macromolecules 35 (17) (2002) 6613.
[25] J. Hyun, D.E. Aspnes, J.J. Cuomo, Macromolecules 34 (2001) 2395.
[26] N.M. Alves, J.F. Mano, E. Balaguer, J.M. Meseguer Duenas, J.L. Gomez Ribelles, Polymer 43 (2002) 4111.
[27] F. Dinelli, H.E. Assender, K. Kirov, O. Kolosov, Polymer 41 (2000) 4285.
[28] W.A. MacDonald, J. Mater. Chem. 14 (2004) 4.
[29] T.P. Davis, in: O Olabisi (Ed.), Handbook of Thermoplastics, Marcel Dekker, New York, 1997.
[30] R.M. Gohil, J. Appl. Polym. Sci. 52 (1994) 925.
[31] N.W. Hayes, G. Beamson, D.T. Clark, D.S.L. Law, R. Raval, Surf. Interface. Anal. 24 (10) (1996) 723.
[32] P.C. Jukes, A. Das, M. Durell, D. Trolley, A.M. Higgins, M. Geoghegan, J.E. MacDonald, R.A.L. Jones, S. Brown, P. Thompson, Macromolecules 38 (2005) 2315.
[33] S.A. Jabarin, Polym. Eng. Sci. 31 (14) (1991) 1071.
[34] B.D. Beake, G.J. Leggett, P.H. Shipway, Surf. Interface Anal. 31 (2001) 39.
[35] S. Paul, Surface Coatings Science and Technology, Wiley Inter Science, New York, 1986.